HHS Public Access

Author manuscript

*Invest Radiol*. Author manuscript; available in PMC 2022 July 01.

Published in final edited form as:

*Invest Radiol*. 2021 July 01; 56(7): 409–416. doi:10.1097/RLI.0000000000000754.

# Navigator-Guided Motion and $B_0$ Correction of $T_2$*-weighted MRI Improves Multiple Sclerosis Cortical Lesion Detection

**Jiaen Liu, PhD**[1,*], **Erin S Beck, MD, PhD**[2,*], **Stefano Filippini, MD**[2,3], **Peter van Gelderen, PhD**[1], **Jacco A de Zwart, PhD**[1], **Gina Norato, ScM**[4], **Pascal Sati, PhD**[2,5], **Omar Al-Louzi, MD**[2], **Hadar Kolb, MD**[2], **Maxime Donadieu, PhD**[2], **Mark Morrison, BA**[2], **Jeff H Duyn, PhD**[1], **Daniel S Reich, MD, PhD**[2]

[1]Advanced MRI Section, National Institute of Neurological Disorders and Stroke (NINDS), National Institutes of Health (NIH), Bethesda, MD, USA

[2]Translational Neuroradiology Section, NINDS, NIH, Bethesda, MD, USA

[3]Department of Neurosciences, Drug, and Child Health, University of Florence, Florence, Italy

[4]Clinical Trials Unit, NINDS, NIH, Bethesda, MD, USA

[5]Department of Neurology, Cedars-Sinai Medical Center, Los Angeles, CA, USA

## Abstract

**Background:** Cortical lesions are common in multiple sclerosis (MS). $T_2$*-weighted ($T_2$*w) imaging at 7 tesla (7 T) is relatively sensitive for cortical lesions, but quality is often compromised by motion and main magnetic field ($B_0$) fluctuations.

**Purpose:** To determine whether motion and $B_0$ correction with a navigator-guided, gradient-recalled echo (GRE) sequence can improve cortical lesion detection in $T_2$*w MRI.

**Materials and methods:** In this prospective study, a GRE sequence incorporating a navigator allowing for motion and $B_0$ field correction was applied to collect $T_2$*w images at 7 T from adults with MS between August 2019 and March 2020. $T_2$*w images were acquired in 1–3 partially overlapping scans per individual and were reconstructed using global average $B_0$ correction ("uncorrected") or motion correction and spatially linear $B_0$ correction ("corrected"). Image quality rating and manual segmentation of cortical lesions were performed on uncorrected and corrected images. Lesions seen on a single scan were retrospectively evaluated on the complementary scan. The association of cortical lesions with clinical disability was assessed. Mixed models were used to determine the effect of correction on lesion detection as well as on the relationship between disability and lesion count.

**Results:** 22 $T_2$*w scans were performed on 11 adults with MS (mean age 49 years, standard deviation 11 years, 8 women). Quality improved for 20/22 scans (91%) after correction. 69 cortical lesions were identified on uncorrected images (median per scan 2, range 0–11) vs. 148 on

**Corresponding author:** Daniel S Reich, 10 Center Drive MSC 1400, Building 10 Room 5C103, Bethesda, MD 20892, USA, daniel.reich@nih.gov, Phone: 301-496-1801, Fax: 301-402-0373.

*Authors contributed equally

Address: 10 Center Dr., Bethesda, Maryland, USA, 20892

corrected images (median per scan 4.5, range 0–25, risk ratio (RR) 2.1, p<0.0001). For low-quality uncorrected scans with moderate-to-severe motion artifact (18/22, 82%), there was an improvement in cortical lesion detection with correction (RR 2.5, p<0.0001), whereas there was no significant change in cortical lesion detection for high-quality scans (RR 1.3, p=0.43).

**Conclusions:** Navigator-guided motion and $B_0$ correction substantially improves overall image quality of $T_2$*w MRI at 7 T and increases its sensitivity for cortical lesions.

### Keywords

multiple sclerosis; cortical lesions; motion correction; 7 tesla; gradient echo MRI

## Introduction

Multiple sclerosis (MS) is an autoimmune demyelinating disease of the central nervous system that involves both the white and gray matter of the brain. White matter lesion formation is associated with disability accrual but does not explain the full range of neurological deficits observed in patients. This gap is partly explained by the presence of cortical gray matter lesions, which begin forming during the first phases of the disease (1, 2). Cortical lesions are associated with cognitive disability, clinical severity, and rapid passage to secondary progression (3–6). Despite growing evidence for the importance of cortical lesions in MS, magnetic resonance imaging (MRI) of pathological cortex is still a challenge, due to poor signal contrast between normal and demyelinated gray matter, small size of lesions, and artifacts (7–9).

$T_2$*-weighted ($T_2$*w) MRI at 7 tesla (7 T) has excellent sensitivity to iron and myelin in brain tissue because of their magnetic susceptibility. At submillimeter resolution, this technique holds promise for in vivo delineation of fine features of brain anatomy such as subcortical structures (10–12), intracortical layers (13, 14), and juxtacortical white matter (or U-fibers) (15). In MS, 7 T $T_2$*w MRI is more sensitive for focal cortical lesions than 3 T double inversion recovery or 3 T $T_1$-weighted ($T_1$w) sequences (8, 16, 17), although new 3 T methods as well as new acceleration methods and deep learning-based synthetic techniques may improve sensitivity at 3 T (18–21). Leukocortical lesions, which involve both the deeper layers of cortex and the juxtacortical white matter, are detectable by a wide variety of MR sequences (22, 23). However, subpial lesions, affecting the more superficial layers of cortex, are rarely seen on clinical MR sequences, but they are notably detected by $T_2$*w imaging at 7 T (24), due in part to the difference in magnetic susceptibility between demyelinated cortex and normal appearing gray matter (25). Nevertheless, a high sensitivity of $T_2$*w MRI to artifacts from head motion and motion-induced magnetic field ($B_0$) fluctuations (26) compromises visualization of cortical lesions.

Various methods have been developed to mitigate the longstanding issue of motion in clinical MRI (27–31). Nevertheless, these methods incompletely address the strong effects of motion-induced $B_0$ changes on 7 T $T_2$*w MRI. Recently, a $T_2$*w gradient-recalled echo (GRE) sequence was proposed as a way to monitor motion-induced $B_0$ changes by acquiring a series of low-resolution images (“navigators”) together with the imaging data, and to use

these to correct for both motion and $B_0$ fluctuation (32). Application of this method is straightforward and does not require the use of additional hardware or scan time.

Here we describe the use of the navigator-guided correction for motion and $B_0$ fluctuation in a clinical application and demonstrate improved image quality and substantially increased cortical lesion detection in MS.

## Materials and Methods

### Study participants

This study was approved by the local institutional review board, and informed consent was obtained from all participants. In a cohort of 64 adults with MS scanned consecutively as part of a longitudinal study, the prevalence and severity of motion and associated $B_0$ changes on $T_2$*-weighted ($T_2$*w) MRI quality at 7 T was retrospectively evaluated. Participants were scanned using uncorrected, traditional $T_2$*w MRI between August 2017 and September 2018. To evaluate the effects of motion and $B_0$ correction of $T_2$*w MRI on image quality and cortical lesion visualization in MS, a navigator-guided $T_2$*w (nav$T_2$*w) GRE sequence (32) and $T_1$w MP2RAGE (Magnetization Prepared 2 Rapid Acquisition Gradient Echoes) (33, 34) were acquired at 7 T prospectively for 11 adults with MS (6 of whom were also part of the 64-participant cohort scanned with the traditional $T_2$*w sequence) scanned consecutively as a part of a pre-existing MS natural history study between August 2019 and March 2020. Expanded Disability Status Scale (EDSS) was determined by a clinician on the day of the MRI. See Table 1 for clinical characteristics of the two cohorts. Inclusion required diagnosis of MS or clinically isolated syndrome, age ≥18, and ability to give informed consent. Individuals with any contraindication to 7 T MRI and pregnant women were excluded.

### MRI acquisition

All MRI scans were performed on a 7 T whole-body research system (Magnetom, Siemens, Erlangen, Germany) equipped with a single-channel transmit and 32-channel receiver array head coil (Nova Medical, Wilmington, MA, USA). Participants' heads were cushioned with standard ear pads, with no specific fixation in the head coil.

Parameters of the traditional $T_2$*w GRE, nav$T_2$*w GRE, and MP2RAGE sequences are summarized in Table 2. In the traditional $T_2$*w GRE sequence acquired for the 64-participant cohort, a 1D navigator in the read-out gradient direction was acquired to correct for average $B_0$ (35). In the nav$T_2$*w GRE sequence, head motion and $B_0$ maps were measured in real time using low-resolution navigator images, which were acquired at two shorter echo times (TE) before the high-resolution $T_2$*w data within each repetition time (TR) period (32). Four echoes were acquired for the high-resolution GRE data in the nav$T_2$*w GRE sequence compared to five in the traditional sequence. This was considered to have a minor effect on the contrast-to-noise ratio, because the early GRE signal had negligible $T_2$*w contrast. Parameters of the navigator acquisition are included in Table 2. Specifically, it utilized an eight-shot 3D echo-planar imaging (EPI) approach with 4×2 parallel imaging factor (in the first and second phase encoding directions, respectively); this

resulted in a 0.6 s volume TR of the navigator images. To provide reference data for the parallel imaging reconstruction of the navigator images, the k-space $k_y$ and $k_z$ coordinates of the accelerated acquisition were shifted in a periodic manner to cover the full k-space while still allowing for high temporal resolution (0.6 s) in motion and $B_0$ measurement (32).

The traditional $T_2$*w GRE and the nav$T_2$*w GRE sequences were acquired in scans measuring 30 mm or 32 mm, respectively, in the superior-inferior dimension. To obtain nearly full supratentorial brain coverage, for each participant in the 64-participant cohort, 3 scans (corresponding to the "top," "middle," and "bottom" portions of the supratentorial brain) were acquired, with an overlap of approximately 2 mm between adjacent scans. For the nav$T_2$*w GRE, in five cases, a single scan was acquired ("top" in one case, "middle" in three cases, and "bottom" in one case); in one case, two partially overlapping scans were acquired ("top" and "middle"); and in the remaining five cases, all three partially overlapping scans were acquired. In total, 22 nav$T_2$*w GRE scans were acquired.

## MRI reconstruction and processing

The navigator images were reconstructed using generalized autocalibrating partially parallel acquisitions (GRAPPA) (36) and kernel size of 3×2×2. Head motion was estimated based on the navigator magnitude (37). $B_0$ distribution in the head frame was calculated using the spatially aligned navigator phase images.

MP2RAGE images were reconstructed using the Siemens research sequence package (Work-in-Progress Package #900B). Images acquired using the traditional $T_2$*w sequence were reconstructed with correction for the average $B_0$ measured in the 1D navigator. Images acquired using the nav$T_2$*w sequence were reconstructed in "uncorrected" and "corrected" modes. Uncorrected images were reconstructed only with compensation for the volume-average $B_0$ fluctuation. Corrected images were reconstructed by compensating for navigator-measured rigid-body motion and spatially linear $B_0$ changes in the k-space of MRI data (32) using the nonuniform Fast Fourier Transform algorithm (38) and an in-house Matlab (Mathworks, Natick, MA, USA) program. Parallel imaging reconstruction of the high resolution data was performed by incorporating the sensitivity maps of the receiver coils in the correction model (32). The receiver sensitivity was extracted from a GRE pre-scan covering the volume of interest (resolution/TE/TR/scan time= isometric 4 mm/3 ms/84 ms/3.8 s).

Magnitude of all $T_2$*w images was calculated as the average of the magnitude images at each TE. $T_2$*w images were aligned to MP2RAGE images using linear coregistration in AFNI (Analysis of Functional Neuroimages, https://afni.nimh.nih.gov).

## Image-quality rating

The prevalence of motion and motion-induced $B_0$ effects on $T_2$*w MRI quality at 7 T was evaluated retrospectively in the 64-participant cohort scanned using a traditional, uncorrected $T_2$*w GRE sequence. A single rater (ESB, with 4 years of MS neuroimaging experience) qualitatively assessed traditional, uncorrected $T_2$*w images and assigned each scan one of the following quality grades: 4 (no motion artifacts), 3 (minimal motion artifacts), 2 (moderate motion artifacts) or 1 (severe motion artifacts). Uncorrected and

corrected individual navT$_2$*w image scans were qualitatively assessed by two raters (OA, with 7 years of MS neuroimaging experience, and HK, with 4 years of MS neuroimaging experience) using the same qualitative scale; see Figure 1 for examples. Raters assessed corrected and uncorrected scans independently, in random order and blinded to correction status, and the two ratings were averaged. Rating of uncorrected and corrected images were not necessarily done in separate sessions.

### Cortical lesion identification

Cortical lesions were identified on the uncorrected and corrected navT$_2$*w images by two raters independently (SF, with 2 years of MS neuroimaging experience, and ESB, with 4 years of MS neuroimaging experience). This evaluation was done in random order, blinded to clinical data and correction status, with at least one week between the analysis of uncorrected and corrected images from the same scan. Cortical lesions were classified as leukocortical, intracortical, or subpial (39). Any lesion identified by only one rater or on only one image type (corrected or uncorrected) was verified using the corresponding T$_1$w MP2RAGE image. Lesions that were not verified on MP2RAGE images were categorized as false positives and were not included in total lesion counts. Following lesion identification on both sets of images, each lesion was evaluated retrospectively on corrected vs. uncorrected images, viewed side-by-side, to determine the impact of the correction on cortical lesion visualization.

### Statistical analysis

To determine the difference in lesion identification due to correction, a Poisson mixed model was fit with lesion count as the outcome and correction status as a fixed effect (Model 1).

> Model 1: $\log(\text{lesion count})_{ij} = \beta_0 + \beta_1 * \text{correction} + b_{0j} + b_{0jk} + e_{ijk}$ , where correction is the fixed effect, i indicates lesion, j indicates scan, k indicates participant and $b_{0j}$ and $b_{0jk}$ are the nested random intercepts for scan and participant, respectively.

To test the effect of correction on lesion count in images with different levels of motion artifact, Model 1 was extended by incorporating quality of uncorrected images (high quality, ≥3 vs low quality, <3) and the interaction between quality and correction as fixed effects (Model 2).

> Model 2: $\log(\text{lesion count})_{ij} = \beta_0 + \beta_1 * \text{correction} + \beta_2 * \text{quality} + \beta_3 * (\text{correction} * \text{quality}) + b_{0j} + b_{0jk} + e_{ijk}$, with correction, quality, and their interaction as fixed effects.

To evaluate the effect of correction on the relationship between lesion count and disability, lesion count was modeled with EDSS, correction, and their interaction as fixed effects (Model 3). Although we assumed that lesions contribute to disability and not vice versa, lesion count was used as the outcome in this model due to the inability to fit a mixed model on an outcome with no variability within patient (i.e., EDSS is the same regardless of scan correction).

Model 3: $\log(\text{lesion count})_{ij} = \beta_0 + \beta_1 * \text{correction} + \beta_2 * \text{EDSS} + \beta_3 * (\text{correction} * \text{EDSS}) + b_{0j} + b_{0jk} + e_{ijk}$, with EDSS, correction and their interaction as fixed effects.

In all models, participant and scan were incorporated as nested random intercepts, and Poisson regression was used to fit all models. Models 1 and 2 were evaluated for total lesions as well as for lesion subtypes (leukocortical and subpial). Results from the Poisson models are presented as relative risks (rate ratios; RR) with 95% confidence intervals. The Mann-Whitney test was used to compare false positive rates in corrected vs. uncorrected scans. Intraclass correlation coefficients (ICCs) were determined using a 2-way model. P-values were considered significant at <0.05.

## Results

### Motion frequently affects 7 T $T_2$*w image quality in MS

In the retrospective cohort of 64 adults with MS scanned with a traditional, non-motion-corrected $T_2$*w GRE sequence acquired in 3 partially overlapping scans, 11 individuals (17%) had at least one scan with a quality rating of 1 (severe motion artifact). For 21 individuals (33%), the worst quality scan was rated 2 (moderate motion artifact), and for 23 individuals (36%) the worst quality scan was rated 3 (minimal motion artifact). All acquired scans were rated 4 (no motion artifact) in only 9 individuals (14%) (Table 3).

### Motion and $B_0$ correction improve $T_2$*w image quality

In the prospective cohort of 11 adults with MS scanned with the nav$T_2$*w sequence, on qualitative review of uncorrected vs. corrected images, we noted improvement in visualization of vasculature, both parenchymal and extra-axial, white matter lesion borders, and cortex-white matter and cortex-cerebrospinal fluid boundaries (Figure 1). Average quality rating was unchanged for 2/22 scans following correction, 12 scans improved in quality by 0.5–1 point, and 8 scans improved by 1.5–2 points (Figures 1, 2). For the uncorrected images, only 4/22 scans (18%) were rated between 3 and 4, versus 21/22 scans (95%) for the corrected images (Figure 2).

### Image correction improves cortical lesion detection

Cortical lesions were identified independently on uncorrected and corrected nav$T_2$*w scans, by 2 raters masked to correction status. The number of cortical lesions identified increased with correction on 16/22 scans (73%), was unchanged on 5/22 scans (22%), and decreased on 1/22 scans (5%). 16/22 uncorrected scans (73%) had at least one cortical lesion, versus 18/22 corrected scans (82%).

69 total confirmed cortical lesions (median 2 per scan, range 0–11) were found on uncorrected images, versus 148 on corrected images (median 4.5 per scan, range 0–25). When a mixed model was used to determine the relationship between the number of lesions identified and correction, the risk ratio (RR) of lesions identified on corrected images to uncorrected images was 2.1 (confidence interval (CI) 1.6–2.8, p<0.0001) (Table 4, Figures 3–4).

When individual lesion subtypes were considered, the effect of correction on lesion identification was significant for both leukocortical lesions (RR 1.7, CI 1.2–2.4, p=0.002) and subpial lesions (RR 3.2, CI 1.8–5.5, p<0.0001). No purely intracortical lesions were identified on either image type.

When divided by quality (high quality: score ≥3 vs low quality: <3), for the 4 scans with high-quality uncorrected images, the number of total cortical lesions identified increased with correction on 2/4 scans (50%) and was unchanged on 2/4 scans (50%) (Figure 4, Table 4). For scans with low-quality uncorrected images, the number of cortical lesions identified increased with correction on 14/18 scans (78%), was unchanged on 3/18 scans (17%), and decreased on 1/18 scans (5%). For high-quality scans, there was no apparent change in lesion count between corrected and uncorrected images (RR 1.3, CI 0.7–2.3, p=0.43), whereas for low-quality scans, there was a significant interaction between lesion count and correction (RR 2.5, CI 1.8–3.4, p<0.0001). However, the interaction between quality and correction was not significant for total lesions or for either lesion subtype (Figure 4, Table 4).

Of putative lesions identified on uncorrected images, 8 out of 77 total lesions identified (10%) were classified as false positives, whereas on corrected images, 20/168 lesions (12%) were false positives (p=0.57). ICC for total cortical lesion number was similar for uncorrected (0.70, CI 0.40–0.86) and corrected (0.65, CI 0.32–0.84) images.

Cortical lesion number per scan was correlated with disability, as measured by EDSS, when using corrected images (slope 1.5, CI 1.2–1.9, p=0.002) and uncorrected images (slope 1.4, CI 1.1–1.8, p=0.01). The interaction between the two slopes was not significant (p=0.47)

### Retrospective review of cortical lesions identified on uncorrected vs corrected navT$_2$*w images

A total of 166 unique cortical lesions were identified after analyzing uncorrected and corrected images: 50 (30%) were identified on both, 98 (59%) were identified only on corrected images, and 18 (11%) were identified only on uncorrected images. All lesions identified on only one set of images were reviewed retrospectively on the other set of images. 11/98 lesions (11%) identified only on corrected images were in retrospect seen clearly on uncorrected images, 42 (43%) were seen less clearly on uncorrected images, and 45 (46%) were not seen on uncorrected images. On the other hand, 17/18 lesions (94%) initially identified only on uncorrected images were clearly seen on corrected images, 1 lesion (6%) was seen less clearly on corrected images, and no lesion was not seen on corrected images (Table 5). Of the 17 lesions clearly seen on corrected images, 13 were lesions centered in the juxtacortical white matter with significant surrounding artifact that often obscured the border of the lesion and/or the cortex-white matter junction (Figure 3D). With correction, these lesions appeared juxtacortical, with less clear cortical involvement, and were not identified as cortical lesions. However, after the retrospective review, these lesions were still considered true cortical lesions, given the difficulty in definitively determining whether there was cortical involvement.

For the 50 lesions identified on both corrected and uncorrected images, we compared lesion appearance on both sets of images. 28/50 lesions (56%) were seen clearly on both sets of images, whereas 22/50 (44%) were seen more clearly on corrected images; none was seen more clearly on uncorrected images.

## Discussion

In this study, we show that motion artifact adversely impacts image quality in most 7 T $T_2$*w scans of people with multiple sclerosis, and that application of a navigator-guided motion and magnetic field ($B_0$) correction algorithm to 7 T $T_2$*w images improves image quality and cortical lesion detection. Qualitatively, correction led to decreased motion artifact over the cortex and a clearer delineation of cortex-cerebrospinal fluid, cortex-white matter, and normal cortex-demyelinated cortex borders. Not surprisingly, the advantage of correction was most evident when there was considerable motion artifact on the uncorrected images. This navigator-guided correction approach can replace a traditional $T_2$*w GRE sequence, without the need for additional motion- or field-measurement hardware or lengthening of scan time.

Nearly all cortical lesions that were identified on corrected but not uncorrected images were confirmed to be true lesions after review of the corresponding $T_1$w MP2RAGE images, suggesting that lesions seen on corrected but not uncorrected images are not due to artifacts of the correction process. Given that some cortical lesions are better seen on $T_2$*w images (34), it is possible that our requirement that lesions identified on only one set of $T_2$*w images be verified on $T_1$w MP2RAGE led to incorrect classification of some lesions as false positives. However, the number of lesions classified as false positive was small (28/245, 11%) and was not different between corrected and uncorrected images, so this limitation is unlikely to have influenced our overall findings. Whereas multiple studies use either $T_1$w or $T_2$*w images to identify cortical lesions at 7 T (4, 20, 24, 40–43), we favor a multicontrast read of both image types for the most sensitive and accurate cortical lesion detection (34), ideally using the nav$T_2$*w method described here.

Of the small number of lesions identified on uncorrected but not corrected images, most were lesions centered in the juxtacortical white matter with adjacent artifact that made determination of cortical involvement difficult. Differentiation between juxtacortical and leukocortical lesions is difficult even on high-quality $T_2$*w images, and accurate identification of each type is greatly improved by the use of $T_1$w images with good cortex-white matter contrast, such as MP2RAGE. Other lesions identified on uncorrected but not corrected images were seen clearly in retrospect on the corrected images and thus were simply missed during the original rating. Relatively low intra- and inter-rater reliability is a known issue in cortical lesion identification (18, 34, 44).

Importantly, there were no lesions identified on uncorrected images that could not be seen in retrospect on the corrected images, meaning that the correction process does not make cortical lesions harder to visualize. There was only one lesion identified only on uncorrected images that was not seen well on the corresponding corrected image; this lesion was small and subtle even on uncorrected images.

Although this study was well-powered to measure the effect of motion and $B_0$ correction on cortical lesion detection, the sample size is nonetheless small, particularly with respect to high-quality scans. In addition, we found a relationship between cortical lesion number and disability consistent with previous studies (4, 40, 45), but due to the small sample size and limitations of our model, further studies will be needed to clarify the strength of this relationship.

Although our study was focused on the utility of motion and $B_0$ correction of $T_2$*w images on cortical lesion identification, it is likely that the methods described here will be beneficial to other applications of $T_2$*w imaging, including assessment of central veins and chronic inflammation in MS lesions, cortical pathology in other diseases, vascular pathology, and cortical anatomy.

Given the pervasive problem of motion on sensitive, high-resolution $T_2$*w scans that we observed in our larger retrospective MS cohort, we expect that the correction method evaluated here will allow more accurate determination of both the clinical implications of cortical lesions and the detection of their accrual over time, especially with the increasing clinical use of 7 T MRI in the MS population.

## Acknowledgments

We acknowledge the staff the NIH Neuroimmunology Clinic for care of and collection of clinical data from the study participants and the staff of the National Institute of Mental Health Functional MRI Fa-cility for help with MR imaging acquisitions. We utilized the NIH high-performance computing cluster (Biowulf) for computation. This research was supported by the Intramural Research Program of the National Institute of Neurological Disorders and Stroke, NIH. Erin Beck was also supported by a Clinician Scientist Development Award and a Career Transition Fellowship from the National Multiple Sclerosis Society.

## References

1. Calabrese M, De Stefano N, Atzori M, et al. Detection of cortical inflammatory lesions by double inversion recovery magnetic resonance imaging in patients with multiple sclerosis. Arch Neurol. 2007;64(10):1416–22. [PubMed: 17923625]
2. Diker S, Has AC, Kurne A, et al. The association of cognitive impairment with gray matter atrophy and cortical lesion load in clinically isolated syndrome. Mult Scler Relat Disord. 2016;10:14–21. [PubMed: 27919482]
3. Calabrese M, Agosta F, Rinaldi F, et al. Cortical lesions and atrophy associated with cognitive impairment in relapsing-remitting multiple sclerosis. Arch Neurol. 2009;66(9):1144–50. [PubMed: 19752305]
4. Harrison DM, Roy S, Oh J, et al. Association of Cortical Lesion Burden on 7-T Magnetic Resonance Imaging With Cognition and Disability in Multiple Sclerosis. JAMA Neurol. 2015;72(9):1004–12. [PubMed: 26192316]
5. Scalfari A, Romualdi C, Nicholas RS, et al. The cortical damage, early relapses, and onset of the progressive phase in multiple sclerosis. Neurology. 2018;90(24):e2107–e18. [PubMed: 29769373]
6. Damasceno A, Damasceno BP, Cendes F. Subclinical MRI disease activity influences cognitive performance in MS patients. Mult Scler Relat Disord. 2015;4(2):137–43. [PubMed: 25787189]
7. Bakshi R, Ariyaratana S, Benedict RH, Jacobs L. Fluid-attenuated inversion recovery magnetic resonance imaging detects cortical and juxtacortical multiple sclerosis lesions. Arch Neurol. 2001;58(5):742–8. [PubMed: 11346369]
8. Kilsdonk ID, Jonkman LE, Klaver R, et al. Increased cortical grey matter lesion detection in multiple sclerosis with 7 T MRI: a post-mortem verification study. Brain. 2016;139(Pt 5):1472–81. [PubMed: 26956422]

9. Geurts JJ, Bo L, Pouwels PJ, et al. Cortical lesions in multiple sclerosis: combined postmortem MR imaging and histopathology. AJNR Am J Neuroradiol. 2005;26(3):572–7. [PubMed: 15760868]
10. Deistung A, Schafer A, Schweser F, et al. High-Resolution MR Imaging of the Human Brainstem In vivo at 7 Tesla. Front Hum Neurosci. 2013;7:710. [PubMed: 24194710]
11. Federau C, Gallichan D. Motion-Correction Enabled Ultra-High Resolution In-Vivo 7T-MRI of the Brain. PLoS One. 2016;11(5):e0154974. [PubMed: 27159492]
12. Thomas BP, Welch EB, Niederhauser BD, et al. High-resolution 7T MRI of the human hippocampus in vivo. J Magn Reson Imaging. 2008;28(5):1266–72. [PubMed: 18972336]
13. Duyn JH, van Gelderen P, Li TQ, et al. High-field MRI of brain cortical substructure based on signal phase. Proc Natl Acad Sci U S A. 2007;104(28):11796–801. [PubMed: 17586684]
14. Fracasso A, van Veluw SJ, Visser F, et al. Lines of Baillarger in vivo and ex vivo: Myelin contrast across lamina at 7T MRI and histology. Neuroimage. 2016;133:163–75. [PubMed: 26947519]
15. Kirilina E, Helbling S, Morawski M, et al. Superficial white matter imaging: Contrast mechanisms and whole-brain in vivo mapping. Sci Adv. 2020;6(41).
16. Nielsen AS, Kinkel RP, Tinelli E, et al. Focal cortical lesion detection in multiple sclerosis: 3 Tesla DIR versus 7 Tesla FLASH-T2. J Magn Reson Imaging. 2012;35(3):537–42. [PubMed: 22045554]
17. Jonkman LE, Klaver R, Fleysher L, et al. Ultra-High-Field MRI Visualization of Cortical Multiple Sclerosis Lesions with T2 and T2*: A Postmortem MRI and Histopathology Study. AJNR Am J Neuroradiol. 2015;36(11):2062–7. [PubMed: 26228878]
18. Beck ES, Gai N, Filippini S, et al. Inversion Recovery Susceptibility Weighted Imaging With Enhanced T2 Weighting at 3 T Improves Visualization of Subpial Cortical Multiple Sclerosis Lesions. Invest Radiol. 2020;55(11):727–35. [PubMed: 32604385]
19. Finck T, Li H, Grundl L, et al. Deep-Learning Generated Synthetic Double Inversion Recovery Images Improve Multiple Sclerosis Lesion Detection. Invest Radiol. 2020;55(5):318–23. [PubMed: 31977602]
20. Fartaria MJ, Sati P, Todea A, et al. Automated Detection and Segmentation of Multiple Sclerosis Lesions Using Ultra-High-Field MP2RAGE. Invest Radiol. 2019;54(6):356–64. [PubMed: 30829941]
21. Eichinger P, Hock A, Schon S, et al. Acceleration of Double Inversion Recovery Sequences in Multiple Sclerosis With Compressed Sensing. Invest Radiol. 2019;54(6):319–24. [PubMed: 30720557]
22. Abdel-Fahim R, Mistry N, Mougin O, et al. Improved detection of focal cortical lesions using 7T magnetisation transfer imaging in patients with multiple sclerosis. Mult Scler Relat Disord. 2014;3(2):258–65. [PubMed: 25878014]
23. Kober T, Granziera C, Ribes D, et al. MP2RAGE multiple sclerosis magnetic resonance imaging at 3 T. Invest Radiol. 2012;47(6):346–52. [PubMed: 22543966]
24. Mainero C, Benner T, Radding A, et al. In vivo imaging of cortical pathology in multiple sclerosis using ultra-high field MRI. Neurology. 2009;73(12):941–8. [PubMed: 19641168]
25. Bian W, Tranvinh E, Tourdias T, et al. In Vivo 7T MR Quantitative Susceptibility Mapping Reveals Opposite Susceptibility Contrast between Cortical and White Matter Lesions in Multiple Sclerosis. AJNR Am J Neuroradiol. 2016;37(10):1808–15. [PubMed: 27282860]
26. Liu J, de Zwart JA, van Gelderen P, et al. Effect of head motion on MRI B0 field distribution. Magn Reson Med. 2018;80(6):2538–48. [PubMed: 29770481]
27. Derbyshire JA, Wright GA, Henkelman RM, Hinks RS. Dynamic scan-plane tracking using MR position monitoring. J Magn Reson Imaging. 1998;8(4):924–32. [PubMed: 9702895]
28. Zaitsev M, Dold C, Sakas G, et al. Magnetic resonance imaging of freely moving objects: prospective real-time motion correction using an external optical motion tracking system. Neuroimage. 2006;31(3):1038–50. [PubMed: 16600642]
29. Aranovitch A, Haeberlin M, Gross S, et al. Prospective motion correction with NMR markers using only native sequence elements. Magn Reson Med. 2018;79(4):2046–56. [PubMed: 28840611]
30. van der Kouwe AJ, Benner T, Dale AM. Real-time rigid body motion correction and shimming using cloverleaf navigators. Magn Reson Med. 2006;56(5):1019–32. [PubMed: 17029223]

31. Tisdall MD, Hess AT, Reuter M, et al. Volumetric navigators for prospective motion correction and selective reacquisition in neuroanatomical MRI. Magn Reson Med. 2012;68(2):389–99. [PubMed: 22213578]
32. Liu J, van Gelderen P, de Zwart JA, Duyn JH. Reducing motion sensitivity in 3D high-resolution T2*-weighted MRI by navigator-based motion and nonlinear magnetic field correction. Neuroimage. 2020;206:116332. [PubMed: 31689535]
33. Marques JP, Kober T, Krueger G, et al. MP2RAGE, a self bias-field corrected sequence for improved segmentation and T1-mapping at high field. Neuroimage. 2010;49(2):1271–81. [PubMed: 19819338]
34. Beck ES, Sati P, Sethi V, et al. Improved Visualization of Cortical Lesions in Multiple Sclerosis Using 7T MP2RAGE. AJNR Am J Neuroradiol. 2018.
35. Ward HA, Riederer SJ, Jack CR Jr., Real-time autoshimming for echo planar timecourse imaging. Magn Reson Med. 2002;48(5):771–80. [PubMed: 12417991]
36. Blaimer M, Breuer FA, Mueller M, et al. 2D-GRAPPA-operator for faster 3D parallel MRI. Magn Reson Med. 2006;56(6):1359–64. [PubMed: 17058204]
37. Thevenaz P, Ruttimann UE, Unser M. A pyramid approach to subpixel registration based on intensity. IEEE Trans Image Process. 1998;7(1):27–41. [PubMed: 18267377]
38. Fessler JAS BP Nonuniform fast Fourier transforms using min-max interpolation. IEEE Transactions on Signal Processing. 2003;51(2):560–74.
39. Bo L, Vedeler CA, Nyland HI, et al. Subpial demyelination in the cerebral cortex of multiple sclerosis patients. J Neuropathol Exp Neurol. 2003;62(7):723–32. [PubMed: 12901699]
40. Nielsen AS, Kinkel RP, Madigan N, et al. Contribution of cortical lesion subtypes at 7T MRI to physical and cognitive performance in MS. Neurology. 2013;81(7):641–9. [PubMed: 23864311]
41. Treaba CA, Granberg TE, Sormani MP, et al. Longitudinal Characterization of Cortical Lesion Development and Evolution in Multiple Sclerosis with 7.0-T MRI. Radiology. 2019;291(3):740–9. [PubMed: 30964421]
42. Ighani M, Jonas S, Izbudak I, et al. No association between cortical lesions and leptomeningeal enhancement on 7-Tesla MRI in multiple sclerosis. Mult Scler. 2020;26(2):165–76. [PubMed: 31573837]
43. Zurawski J, Tauhid S, Chu R, et al. 7T MRI cerebral leptomeningeal enhancement is common in relapsing-remitting multiple sclerosis and is associated with cortical and thalamic lesions. Mult Scler. 2020;26(2):177–87. [PubMed: 31714181]
44. Faizy TD, Thaler C, Ceyrowski T, et al. Reliability of cortical lesion detection on double inversion recovery MRI applying the MAGNIMS-Criteria in multiple sclerosis patients within a 16-months period. PLoS One. 2017;12(2):e0172923. [PubMed: 28235075]
45. Calabrese M, Poretto V, Favaretto A, et al. Cortical lesion load associates with progression of disability in multiple sclerosis. Brain. 2012;135(Pt 10):2952–61. [PubMed: 23065788]

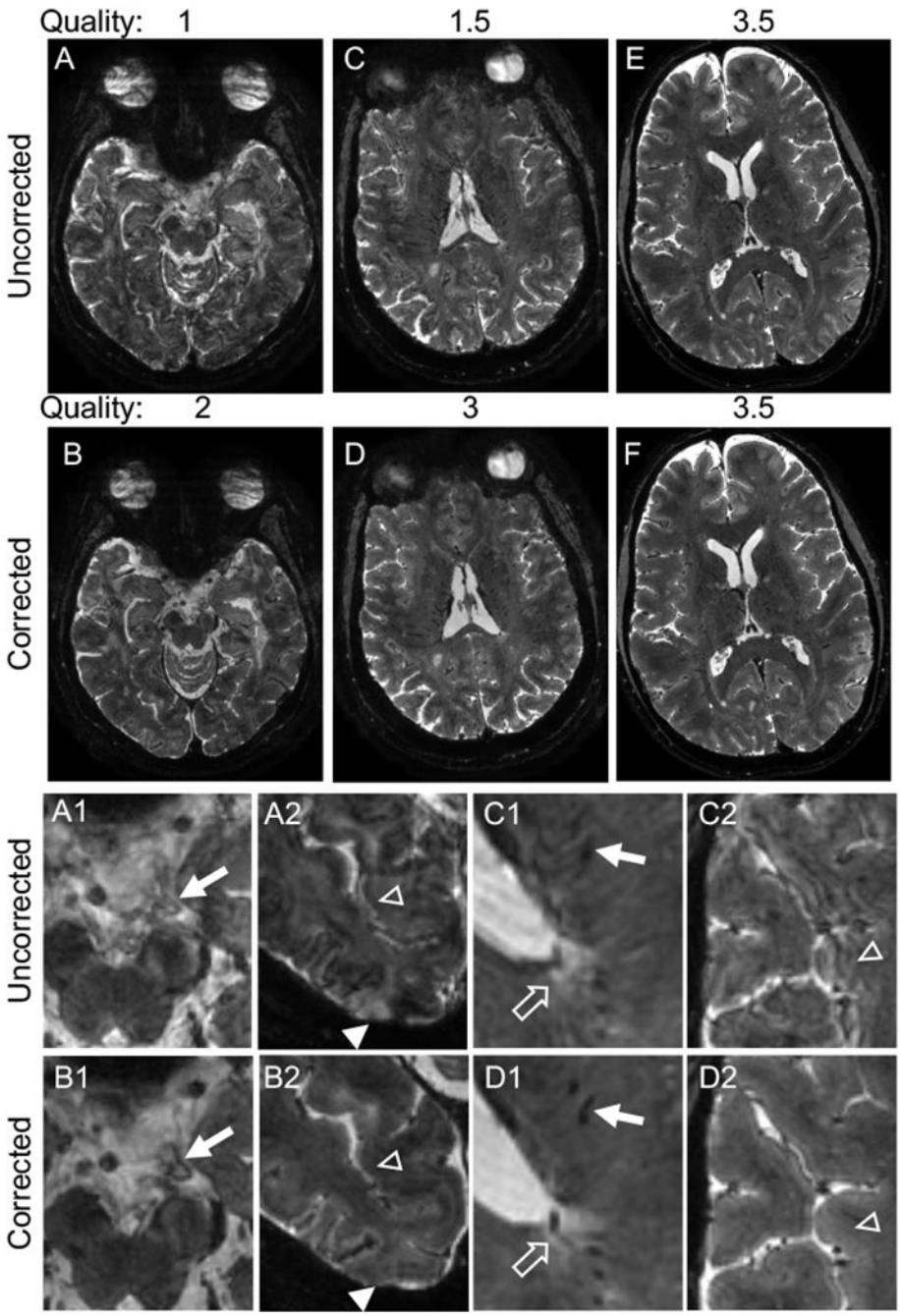


**Figure 1.**

Navigator-guided motion and $B_0$ correction improves the quality of $T_2$*-weighted images. (A–D) Examples of uncorrected scans with a low-quality score (average of 2 ratings: 1 (A) and 1.5 (C)), which improved to 2 (B) and 3 (D) respectively after correction. (E–F) Example of a higher quality uncorrected scan (average rating 3.5) and corresponding corrected image with equal quality. All images are in the axial plane. Images in the bottom two rows are magnified portions of the images from the top rows. Correction improves visualization of vasculature (A1 vs. B1, C1 vs. D1, arrows) and clarity of the border of white

matter lesions (C1 vs. D1, unfilled arrows). Correction also eliminates hyperintense artifact in the cortex (A2 vs. B2, filled arrowheads) and alternating hyperintense/hypointense artifact along the cortex (A2 vs. B2, C2 vs. D2, unfilled arrowheads), with resulting improvement in clarity of the cortex-white matter border (C2 vs. D2). Quality ratings: 1 – severe motion artifacts, 2 – moderate motion artifacts, 3 – minimal motion artifacts, 4 – no motion artifacts.

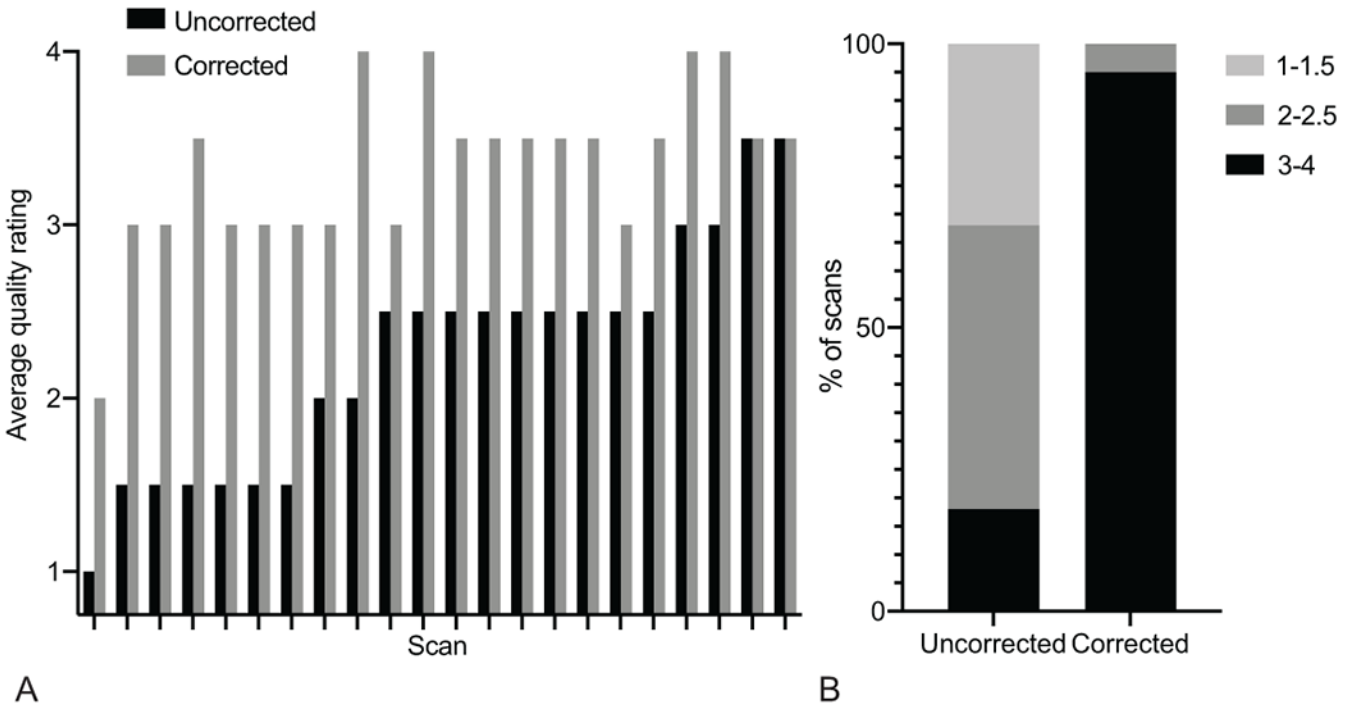


**Figure 2.**

Correction of navigator-guided $T_2$*-weighted images improves quality rating. (A) Average quality ratings of all 22 scans, sorted by the quality rating of the uncorrected scan. (B) Percentage of scans in groups of different quality rating. Quality ratings: 1 – severe motion artifacts, 2 – moderate motion artifacts, 3 – minimal motion artifacts, 4 – no motion artifacts.

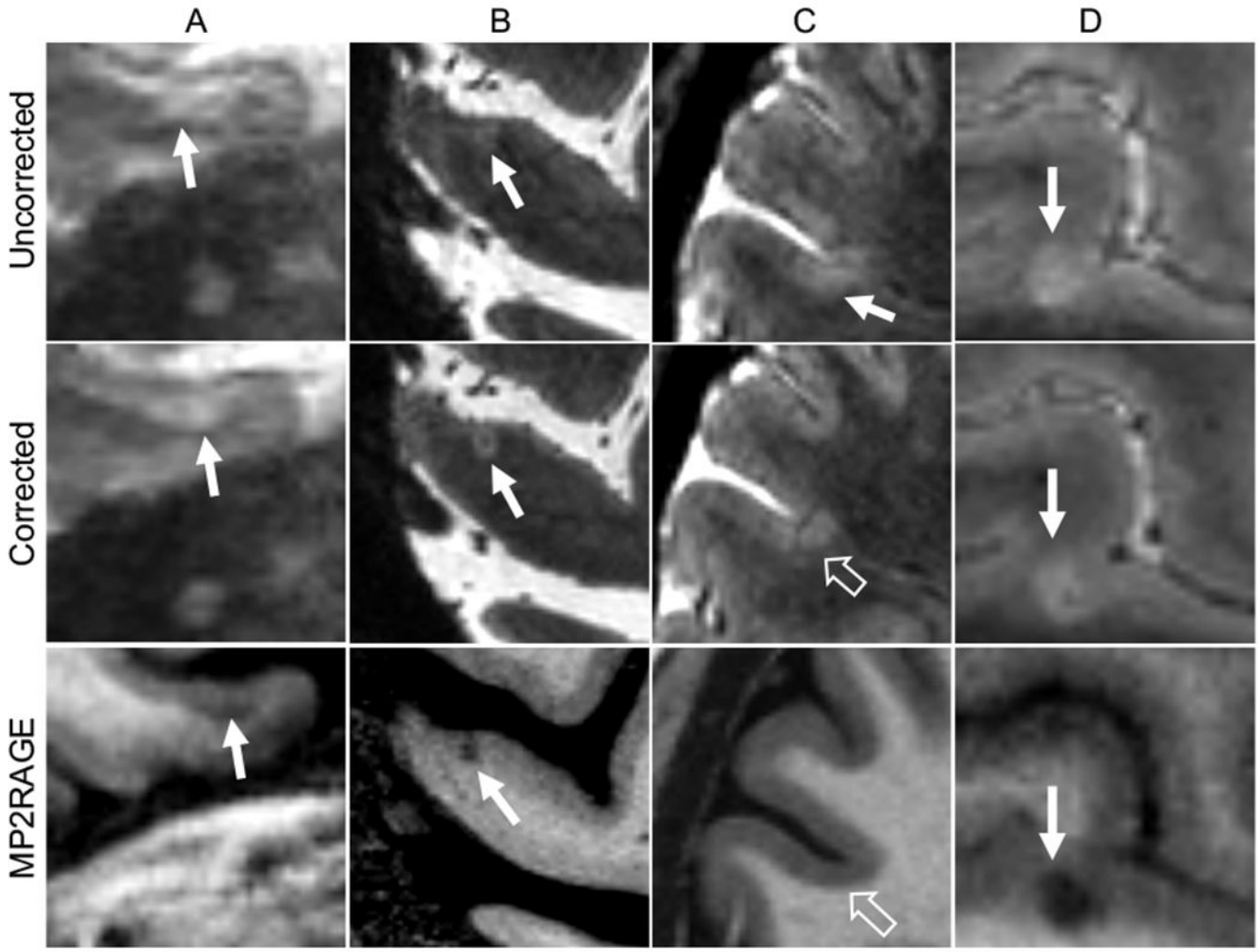


**Figure 3.**

Examples of cortical lesion appearance on corrected vs. uncorrected navigator-guided $T_2$*-weighted gradient recalled echo images. (A, B) Examples of leukocortical (A) and subpial (B) lesions (solid arrows) that were not clearly seen on uncorrected images but were identified on corrected images and were confirmed as lesions on $T_1$-weighted images. (C) Example of a false-positive lesion identified on an uncorrected scan (solid arrow) that was not seen on the corrected scan or corresponding $T_1$-weighted image (unfilled arrows), likely caused by motion artifact in the uncorrected image. (D) Example of a lesion (solid arrows) that was identified on uncorrected but not corrected images, possibly due to artifact in the overlying cortex on the uncorrected images, giving the appearance of more substantial cortical involvement. MP2RAGE= Magnetization Prepared 2 Rapid Acquisition Gradient Echoes

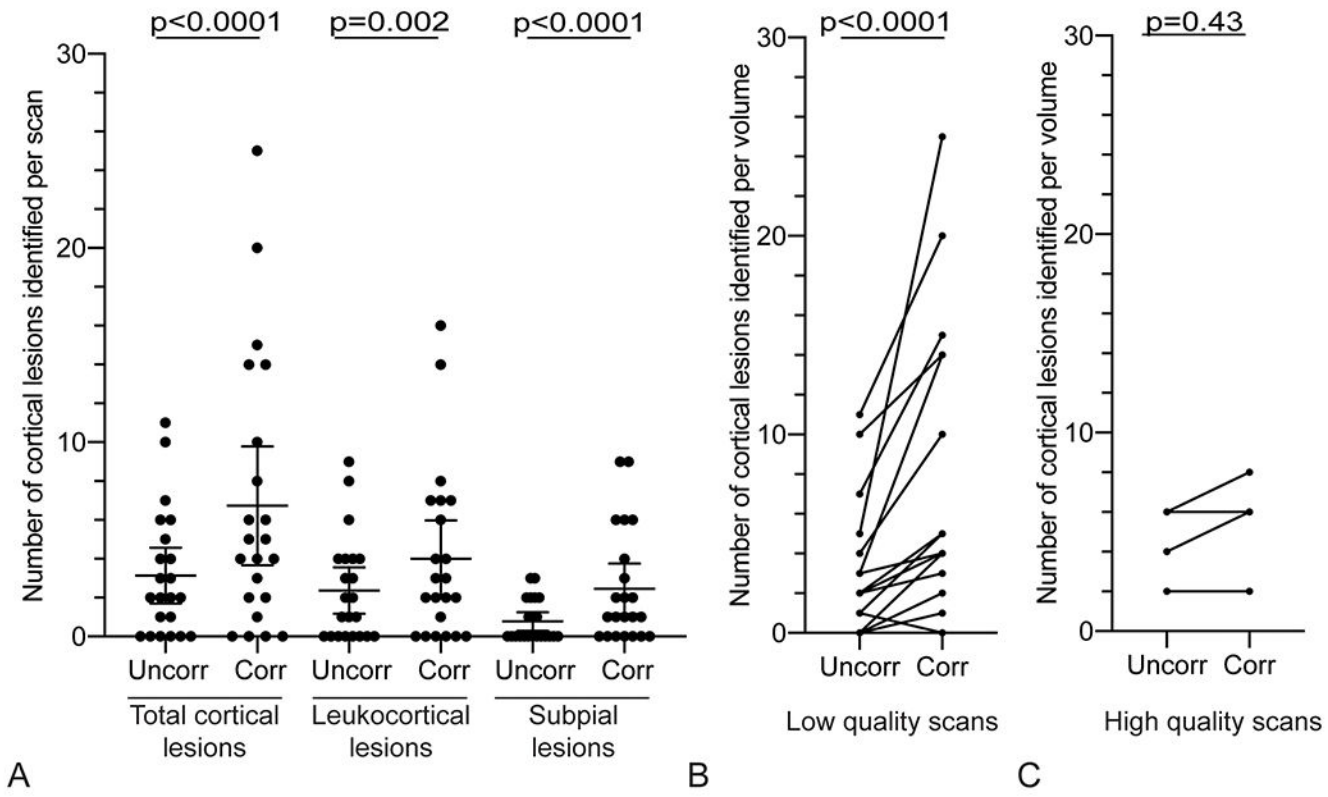


**Figure 4.**

More cortical lesions are identified on navigator-guided $T_2$*w images that have undergone motion and $B_0$ correction. (A) More total cortical lesions, leukocortical lesions, and subpial lesions were identified on corrected images ("Corr") compared to the respective uncorrected images ("Uncorr"). (B) The number of cortical lesions identified in cases with low-quality uncorrected images (average rating <3) increased with correction in 14/18 scans (78%), vs an increase in cortical lesion identification in 2/4 cases (50%) with high-quality uncorrected scans (average rating ⩾3) (C). Quality ratings: 1 – severe motion artifacts, 2 – moderate motion artifacts, 3 – minimal motion artifacts, 4 – no motion artifacts.

**Table 1.**

Clinical characteristics

| | **Traditional $T_2$*w GRE cohort** | **nav$T_2$*w GRE cohort** |
|---|---|---|
| Sex, women/men | 40/24 | 8/3 |
| Age (years), mean ± standard deviation | 49 ± 11 | 49 ± 11 |
| Years since symptom onset, mean ± standard deviation | 14 ± 11 | 19 ± 10 |
| Clinical subtype | | |
| Clinically isolated syndrome | 0 | 1 |
| Relapsing-remitting | 45 | 7 |
| Secondary progressive | 15 | 2 |
| Primary progressive | 4 | 1 |
| Expanded Disability Status Score, median (range) | 2 (0–7.5) | 2.5 (0–7) |

$T_2$*w GRE = $T_2$*-weighted gradient recalled echo

**Table 2.**

MRI parameters

| Parameters | navT$_2$*w GRE | Navigator | Traditional T$_2$*w GRE | MP2RAGE |
|---|---|---|---|---|
| Voxel size (mm$^3$) | 0.5$^3$ | 6×5.625×2.5 | 0.5$^3$ | 0.5$^3$ |
| FOV (mm$^3$) | 240×180×32 | 240×180×30 | 240×168×30 | 224×168×112 |
| Slice oversampling (%) | 25 | 33 | 0 | 7.1 |
| Spatial encoding | 3D | 3D | 2D | 3D |
| Acquisition plane | Axial | Axial | Axial | Axial |
| TE (ms) | 18, 29.48, 40.96, 52.44 | 4.31, 8.95 | 11.4, 22.5, 33.6, 44.7, 55.8 | 3.02 |
| TI (ms) | N/A | N/A | N/A | 800/2700 |
| TR (ms) | 74 | 74 | 4095 | 6000 |
| Flip angle (°) | 10 | 10 | 70 | 4/5 |
| Pixel bandwidth (Hz) | 104 | 1250 | 104 | 237 |
| Parallel imaging | 3×1 | 4×2 | 2 | 3 |
| Scan time (min:sec) | 11:50 | 0.6 sec | 11:26 | 10:32 |
| No. of repetitions | 1 | N/A | 1 | 4 |

Note: navT$_2$*w GRE=navigator-guided T$_2$*-weighted gradient recalled echo sequence, MP2RAGE= Magnetization Prepared 2 Rapid Acquisition Gradient Echoes

**Table 3.**

Prevalence of motion artifact on traditional $T_2$*w images.

| Quality score | All scans (%) | Worst quality scan per individual (%) |
|---|---|---|
| 1 - severe motion artifacts | 19 (10%) | 11 (17%) |
| 2 - moderate motion artifacts | 44 (24%) | 21 (33%) |
| 3 - minimal motion artifacts | 70 (37%) | 23 (36%) |
| 4 - no motion artifacts | 54 (29%) | 9 (14%) |

**Table 4.**

Prospective identification of cortical lesions on uncorrected vs. corrected images.

| | Uncorrected | | Corrected | | Ratio of corrected to >uncorrected lesions | | Quality interaction |
|---|---|---|---|---|---|---|---|
| | **Total** | **Median per scan (range)** | **Total** | **Median per scan (range)** | **Risk ratio (confidence interval)** | **P value** | **P value** |
| All scans | | | | | | | |
| Total cortical | 69 | 2 (0–11) | 148 | 4.5 (0–25) | 2.1 (1.6-2.8) | <0.0001 | 0.062 |
| Leukocortical | 52 | 1.5 (0–9) | 88 | 2.5 (0–16) | 1.7 (1.2-2.4) | 0.002 | 0.17 |
| Subpial | 17 | 0 (0–3) | 54 | 1 (0–9) | 3.2 (1.8-5.5) | <0.0001 | 0.37 |
| High quality scans (quality ≥ 3) | | | | | | | |
| Total cortical | 18 | 5 (2–6) | 22 | 6 (2–8) | 1.3 (0.7-2.3) | 0.43 | |
| Leukocortical | 13 | 3.5 (0–6) | 15 | 3 (2–7) | 1.1 (0.5-2.2) | 0.85 | |
| Subpial | 5 | 1 (0–1) | 7 | 1.5 (0–4) | 2.0 (0.6-6.7) | 0.26 | |
| Low quality scans (quality < 3) | | | | | | | |
| Total cortical | 51 | 2 (0–11) | 126 | 4 (0–25) | 2.5 (1.8-3.4) | <0.0001 | |
| Leukocortical | 39 | 1 (0–9) | 73 | 2.5 (0–16) | 1.9 (1.3-2.8) | <0.001 | |
| Subpial | 12 | 0 (0–3) | 47 | 1 (0–9) | 3.5 (1.9-6.6) | <0.0001 | |

**Table 5.**

Retrospective evaluation of cortical lesions

| | Identified on uncorrected | Identified on corrected | Identified on both |
|---|---|---|---|
| Lesions identified prospectively | 18 | 98 | 50 |
| | Retrospective evaluation on complementary images (n, %) | | Evaluation on uncorrected images (n, %) |
| Seen clearly | 17, 94% | 11, 11% | 28, 56% |
| Seen less well | 1, 6% | 42, 43% | 22, 44% |
| Not seen | 0, 0% | 45, 46% | NA |